Strategy for improved NH_2 detection in combustion environments using an Alexandrite laser

Brackmann, Christian; Zhou, Bo; Samuelsson, Per; Alekseev, Vladimir A.; Konnov, Alexander A.; Li, Zhongshan; Aldén, Marcus

Published in:
Spectrochimica Acta Part A: Molecular and Biomolecular Spectroscopy

DOI:
10.1016/j.saa.2017.05.002

2017

Document Version:
Publisher's PDF, also known as Version of record

Spectrochimica Acta Part A: Molecular and Biomolecular Spectroscopy 184 (2017) 235–242

Contents lists available at ScienceDirect

Spectrochimica Acta Part A: Molecular and Biomolecular Spectroscopy

journal homepage: www.elsevier.com/locate/saa

Strategy for improved NH_2 detection in combustion environments using an Alexandrite laser

Christian Brackmann *, Bo Zhou, Per Samuelsson, Vladimir A. Alekseev, Alexander A. Konnov, Zhongshan Li, Marcus Aldén

Division of Combustion Physics, Lund University, Box 118, SE-221 00 Lund, Sweden

ARTICLE INFO

Article history:
Received 3 February 2017
Received in revised form 28 April 2017
Accepted 2 May 2017
Available online 4 May 2017

Keywords:
NH_2 radical
Laser-induced fluorescence
Combustion

ABSTRACT

A new scheme for NH_2 detection by means of laser-induced fluorescence (LIF) with excitation around wavelength 385 nm, accessible using the second harmonic of a solid-state Alexandrite laser, is presented. Detection of NH_2 was confirmed by identification of corresponding lines in fluorescence excitation spectra measured in premixed NH_3-air flames and on NH_2 radicals generated through NH_3 photolysis in a nonreactive flow at ambient conditions. Moreover, spectral simulations allow for tentative NH_2 line identification. Dispersed fluorescence emission spectra measured in flames and photolysis experiments showed lines attributed to vibrational bands of the NH_2 $A^2A_1 \leftarrow X^2B_1$ transition but also a continuous structure, which in flame was observed to be dependent on nitrogen added to the fuel, apparently also generated by NH_2. A general conclusion was that fluorescence interferences need to be carefully considered for NH_2 diagnostics in this spectral region. Excitation for laser irradiances up to 0.2 GW/cm^2 did not result in NH_2 fluorescence saturation and allowed for efficient utilization of the available laser power without indication of laser-induced photochemistry. Compared with a previously employed excitation/detection scheme for NH_2 at around 630 nm, excitation at 385.7 nm showed a factor of ~15 higher NH_2 signal. The improved signal allowed for single-shot NH_2 LIF imaging on centimeter scale in flame with signal-to-noise ratio of 3 for concentrations around 1000 ppm, suggesting a detection limit around 700 ppm. Thus, the presented approach for NH_2 detection provides enhanced possibilities for characterization of fuel-nitrogen combustion chemistry.

1. Introduction

With a large part of energy production based on combustion and increased attention to limited resources as well as global warming concerning fossil-fuel utilization, interest in renewable, biomass-derived, nitrogen-containing fuels has increased [1]. This makes improved understanding of fuel-nitrogen conversion in combustion highly relevant and insights into these processes for development and verification of kinetic mechanisms require accurate experimental data. Fuel-nitrogen chemistry in combustion can be characterized by two reaction paths, involving oxidation of hydrogen cyanide (HCN) or ammonia (NH_3) [2]. The amidogen (NH_2) radical is a key species in the ammonia oxidation path and also an important component in the thermal de-NO_x process [2,3]. Thus, experimental data on NH_2 are crucial for understanding fuel-nitrogen conversion in combustion.

Laser-based techniques offer powerful non-intrusive methods with high temporal and spatial resolution advantageous for characterization of combustion processes [4]. The laser-induced fluorescence (LIF) technique provides specific detection with high sensitivity for many combustion-relevant species and allows for planar and in some cases also volumetric imaging [5]. Laser-based methods have been readily developed and applied for detection of species involved in fuel-nitrogen chemistry, including diatomic nitrogen radicals such as NH [6,7] and CN [8]. Investigations have also been carried out monitoring more complex molecules containing three or more atoms such as HCN [9], NH_3 [10], and NCN [11].

The NH_2 radical has a wide absorption spectrum covering the spectral range 290–830 nm for transitions in the $A^2A_1 \leftarrow X^2B_1$ system [12,13]. The NH_2 ground state corresponds to a bent molecular configuration whereas the excited state is close to linear and the spectrum consists of multiple bands of the bending vibrational mode. Bands are assigned by vibrational quantum numbers v_1, v_2, and v_3 using notation (v_1,v_2,v_3) where quantum number v_2 represents the bending vibration while quantum numbers v_1 and v_3 represent symmetric and anti-symmetric stretch vibrations, respectively. Measurements of NH_2 under combustion conditions have been made using absorption spectroscopy, for example in NH_3-O_2 flames at low as well as atmospheric pressure [14,15]. In addition, sensitive detection of NH_2 has been achieved in shock-tube experiments using a frequency modulation technique [16]

* Corresponding author.
E-mail address: christian.brackmann@forbrf.lth.se (C. Brackmann).

http://dx.doi.org/10.1016/j.saa.2017.05.002

and in NH_3-doped CH_4-air flames using intracavity absorption spectroscopy [17]. The absorption studies were made at wavelengths around 600 nm probing the A^2A_1-X^2B_1 (0,9,0) NH_2 vibrational band. Excitation in this wavelength regime has also been employed for LIF measurements of NH_2 in hydrocarbon flames at low pressure, either seeded with nitrogen compounds, such as NH_3, to the reactants [6] or by employing NO_2 as additional oxidant [18]. In addition, such LIF measurements of NH_2 have been made in NH_3 flames at atmospheric pressure by Copeland et al. who investigated NH_2 detection using LIF with excitation of several vibrational bands covering wavelengths from 570 to 660 nm [19]. Furthermore, NH_2 LIF measurements in $NH_3/N_2O/N_2$ and $H_2/N_2O/N_2$ flames at atmospheric pressure have been made using a krypton ion laser at 647 nm [20]. In these previous studies LIF has been employed for single-point measurements of NH_2 and to the authors knowledge no fluorescence imaging has been attempted so far.

This work presents an approach to NH_2 detection in flames by means of LIF with excitation at shorter wavelengths in the ultraviolet-blue regime. Efficient excitation can be achieved by probing the $A^2A_1(0,19,0) \leftarrow X^2B_1(0,0,0)$ transitions at wavelengths around 385 nm combined with detection above 400 nm. While tunable dye lasers allow for excitation at arbitrary wavelengths in the ultraviolet range, the use of fixed-frequency solid-state lasers might be beneficial due to higher power and ease of operation. A typical example is excitation of formaldehyde using the 355 nm third harmonic of a conventional Nd:YAG laser [21]. In this case, NH_2 excitation around 385 nm can be achieved using the second harmonic of a powerful solid-state tunable Alexandrite laser [22]. This laser has proven to be advantageous for detection of CH [23] and HCO [24] radicals due to its longer pulse duration compared with the Nd:YAG dye laser systems often used for combustion diagnostics. The proposed NH_2 excitation scheme is characterized in terms of spectroscopy and species specificity in flames as well as a NH_2 gas flow generated by laser-induced photolysis of NH_3. The NH_2 LIF signal strength is compared with that obtained for excitation in the visible regime, the potential influence of photochemical effects is addressed, and NH_2 planar LIF imaging is investigated.

2. Experimental

Two laser systems were used for NH_2 LIF measurements using excitation around 385 nm. Primarily the second harmonic of a linear cavity tunable Alexandrite laser (101-PAL, Light Age Inc.) operating at 10 Hz repetition rate, with a pulse duration of typically 70 ns, a linewidth around 2.5 cm^{-1}, and output pulse energy of about 70 mJ was employed. Measurements were also made using a Nd:YAG (Quanta-Ray PRO 250-10, Spectra Physics) pumped dye laser (Cobra Stretch-G-2400, Sirah) operated using Rhodamine 610 generating a tunable beam in the wavelength range 600–635 nm. The red beam was combined with the 1064 nm fundamental of the Nd:YAG laser in a frequency-mixing crystal to generate light in the wavelength range 385–390 nm. The dye laser system had a repetition rate of 10 Hz, pulse duration of 8 ns and the maximum output pulse energy at 385–390 nm was 15 mJ. The linewidth of the beam obtained by frequency mixing was measured to 1.7 cm^{-1}. For comparison with previous work on NH_2 detection by LIF [19] with excitation at 630 nm, a similar approach was also carried out using the dye laser output beam directly without frequency mixing. In addition to detection in a flame, NH_2 was also generated by means of ultraviolet laser photolysis of NH_3 mixed with an Argon flow at room temperature. The 213 nm fifth harmonic of a Nd:YAG laser (Brilliant B, Quantel), repetition rate 10 Hz and pulse duration 5 ns, was used for photodissociation of NH_3 with a pulse energy of 6 mJ. A schematic of the experimental setup with lasers, optics, burner, and detectors is shown in Fig. 1.

In most investigations the laser beams were focused into sheets using an f = +200 mm cylindrical lens. However, the NH_2 excitation at 630 nm required focusing with a spherical lens of f = +200 mm in order to achieve a sufficient signal. For direct comparison a set of measurements were also made with the 385 nm Alexandrite laser beam focused by the spherical lens. For imaging, the Alexandrite laser beam was focused into a ~20 mm high sheet using a cylindrical lens of f = −40 mm combined with a spherical lens of f = +200 mm.

The signals were detected with intensified CCD cameras (Princeton Instruments, PI-MAX). For imaging measurements an f = 50 mm objective (Nikkor f/1.2) was mounted on the camera together with extension tubes to obtain suitable image magnification. Long-pass filters GG400 and RG645 (Schott AG) were used to suppress light at the laser wavelength for excitation of NH_2 at 385 and 630 nm, respectively. Dispersed fluorescence emission spectra were acquired using an f = 60 mm UV condenser lens (B. Halle) focusing fluorescence on the slit of an f = 500 mm spectrometer (Acton SpectraPro 2500, 1200 grooves/mm grating, blazed at 300 nm) for measurements in flames and an f = 150 mm spectrometer (Acton SpectraPro 150, grating 300 grooves/mm grating) for photolysis measurements.

Measurements were made in an NH_3-air flame stabilized on a burner (Holthuis & Associates) consisting of a 60 mm porous bronze plug with a 10 mm diameter central hole. Mixtures of NH_3-air and CH_4-air were independently fed into the central hole and the surrounding porous plug, respectively. An NH_3-air jet flame of equivalence ratio $\Phi = 1.4$ was stabilized above the hole while a stoichiometric CH_4-air co-flow

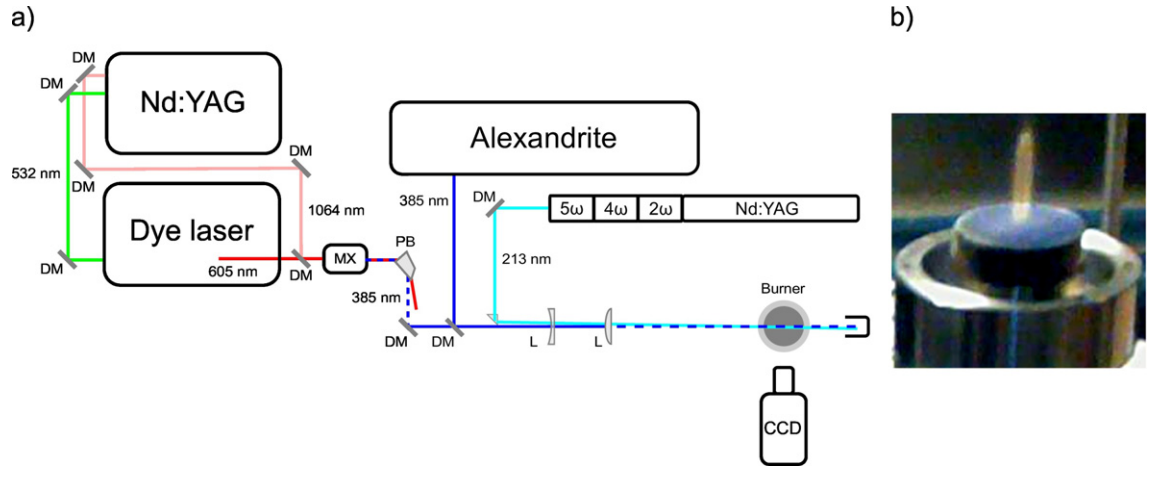

Fig. 1. a) Experimental setup showing the arrangement of lasers, burner, detector and optics. NH_2 LIF was primarily measured using the 385 nm beam from an Alexandrite laser. A continuously tunable beam at the same wavelengths was obtained from a Nd:YAG/dye laser (left). The fifth harmonic of an additional Nd:YAG laser (right) was used to generate NH_2 by means of NH_3 photolysis. Abbreviations: dichroic mirror (DM), Pellin-Broca prism (PB), lens (L), mixing crystal (MX). b) Photo of premixed NH_3-air jet flame of equivalence ratio $\Phi = 1.4$.

pilot flame was operated at the porous plug. The jet flows of NH_3 and air were 0.26 l/min and 0.69 l/min, respectively, resulting in an exit flow velocity of 20 cm/s. The surrounding pilot flame was supplied with 1.2 l/min of CH_4 and 11.2 l/min of air, which resulted in an exit velocity of 7.5 cm/s for the porous plug. All flows were regulated by mass-flow controllers (Bronkhorst). The flame configuration is shown in the photo of Fig. 1b where it can be seen that the jet flame exhibits yellow chemiluminescence, mainly attributed to emission from excited NO_2.

Rotational transitions within an NH_2 vibrational band are designated using rotational quantum numbers N, K_a, and K_c in notation N_{KaKc} where N is the quantum number for angular momentum excluding electron spin while K_a and K_c represent rotational quantum numbers for rotations around axes a and c, aligned perpendicular to and coinciding with the plane of the molecule, respectively. The transitions in vibrational bands can be further categorized into sub-bands defined by the selection rules; transitions for which $K_a = 0$ in the excited state are referred to as Σ sub-bands while transitions for which $\Delta K_a = \pm 1$ are categorized as Δ sub-bands. Further details on NH_2 spectroscopy and spectroscopic notation are given in refs [12,25]. The rotational structure of the investigated NH_2 (0,19,0)Σ and (0,19,0)Δ bands was simulated using the PGOPHER software [26]. Molecular constants for the ground state were adopted from the work of Birss et al. [27] and parameters for the excited state were retrieved from Xin et al. [13].

3. Results & Discussion

Fig. 2a shows a fluorescence excitation spectrum measured in an NH_3-air flame when scanning the dye laser from 385 to 390 nm and detecting fluorescence at wavelengths above 400 nm. A complex spectrum containing lines superimposed on a continuous structure can be observed. The electronic absorption spectrum of NH_2 was analyzed by Dressler and Ramsay [12] and additional rotational-vibrational bands have been studied by Xin et al. [13] showing that the NH_2 (0,19,0)Σ and (0,19,0)Δ bands are located in this spectral region. A spectrum of NH_2 produced via photolysis of NH3 at ambient conditions using the 213 nm beam of the Brilliant B Nd:YAG laser is displayed in Fig. 2b and shows a clearer line structure with a lower continuous background. Rotational lines in the photolysis spectrum can be readily identified in the flame spectrum as well, confirming that a large part of the flame fluorescence originates from NH_2. The continuous background is likely due to unresolved rotational line structure of NH_2 as it also appears in the photolysis spectra where the number of fluorescent species is limited. At elevated temperature in the flame, the line structure becomes more complex due to population of a higher number of ro-vibrational states, which could explain the higher continuous background level of the flame spectrum in Fig. 2a. Copeland et al. [19] has reported on an unidentified fluorescence contribution for an NH_2 excitation spectrum of the $A^2A_1(0,8,0)\Sigma \leftarrow X^2B_1(0,0,0)$ band measured in flame and tentatively assigned it to NH_2 hot bands.

A PGOPHER simulation of the rotational structure of the NH_2 $A^2A_1(0,19,0)\Sigma \leftarrow X^2B_1(0,0,0)$ bands for temperature 300 K and a Gaussian lineshape of width (FWHM) 1.8 cm^{-1} is displayed in Fig. 2c. The PGOPHER model predicted rotational energy levels for the NH_2 ground state [12] as well as line positions for the (0,19,0)Σ and (0,19,0)Δ bands presented by Xin et al. [13]. In addition, peaks observed in the simulated spectrum of Fig. 2c can also be identified in the fluorescence excitation spectrum in Fig. 2b. A spectrum simulated at higher temperature, 1500 K, contains more lines and spectral overlap results in a somewhat higher continuous background, although not of the same magnitude as observed in the flame spectrum of Fig. 2a. However, at flame temperature additional vibrational levels, not accounted for by the PGOPHER simulation, will be populated and make the spectrum more complex as indicated in Fig. 2a. Moreover, it should be noted that the PGOPHER model represents an absorption process and does not include effects on the fluorescence signal such as quantum yield, saturation of individual lines, and line broadening. The simulations suggest that the rather

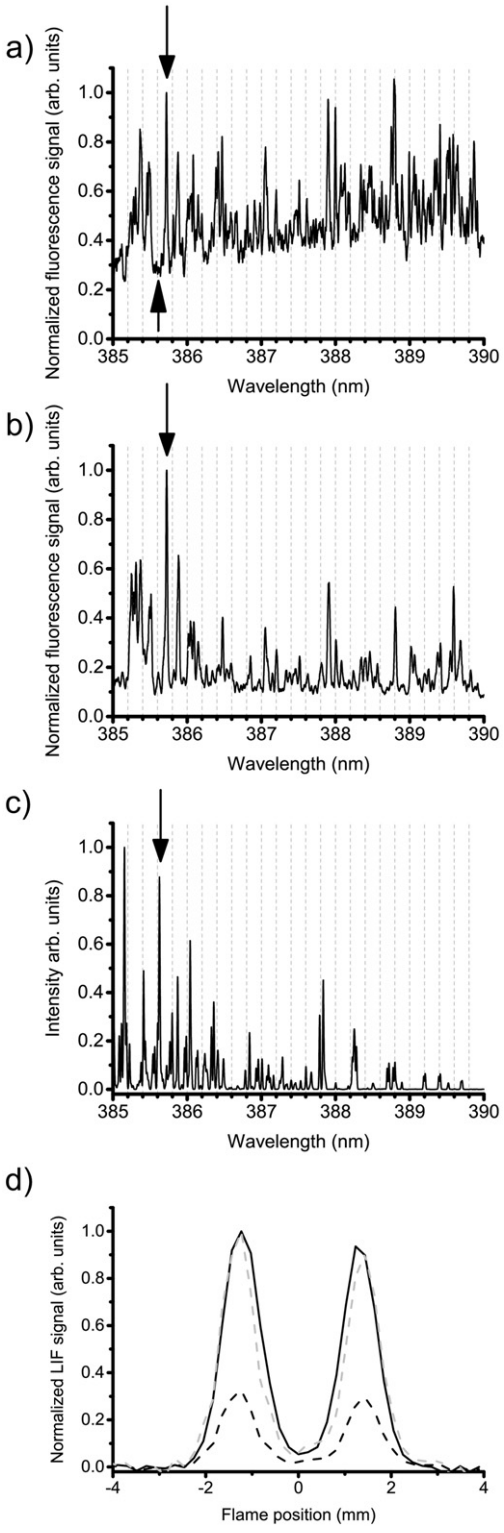

Fig. 2. Excitation scan fluorescence spectra measured in a) NH_3-air flame b) gas jet of NH_3-Argon mixture in which NH_3 is dissociated by UV photolysis. The upper arrow indicates a line at 385.7 nm identified for best NH_2 detection in this range; the lower arrow in (a) indicates a position for excitation at the continuous background level of the flame spectrum. c) PGOPHER simulation of rotational structure in the NH_2 A^2A_1-X^2B_1 (0,19,0) band at 300 K and 1 atm. The rotational lines in the photolysis spectrum can be attributed to NH_2 and can also be identified in the flame spectrum. d) Fluorescence profiles measured across the flame for excitation at the 385.7 nm peak (black solid) and at the background level (black dashed) indicated by the arrows in (a). Scaling the profile measured for excitation at the background level to the same magnitude as the one measured at the peak position, plotted with grey dashed line, shows that the profiles have similar shape.

distinct spectral line at 385.7 nm, indicated by arrow in Fig. 2a–c, corresponds to the two spin components of the 3_{03} $A^2A_1(0,19,0)\Sigma \leftarrow 4_{13}$ $X^2B_1(0,0,0)$ NH_2 transition, labelled using rotational quantum numbers N, K_a, and K_c in notation N_{KaKc} [12].

Fig. 2d shows fluorescence profiles measured in a flame for excitation at the strong peak observed at 385.7 nm and at the continuous background level of the excitation spectrum, indicated in Fig. 2a by the upper and lower arrow, respectively. The profiles measured for excitation at the peak and at the background level, plotted using a black solid and dashed lines, respectively, have similar shape. This is shown by the dashed grey profile in Fig. 2d, which is the profile measured at the background level scaled to the same magnitude as the solid black one measured at the peak of the spectrum. The resemblance in shape supports the interpretation that the signal obtained for excitation at the background level of the flame spectrum, cf. Fig. 2a, is a contribution from NH_2.

An image of spatially resolved and spectrally dispersed fluorescence detected with the Alexandrite laser wavelength tuned to 385.7 nm is shown in Fig. 3a.

The vertical and horizontal axes of the image represent measurement position along the horizontal laser sheet propagating across the flame cone and fluorescence wavelength, respectively. The conical shape of the flame results in a region of unburned reactants in the middle of the image and flame reaction zones above and below, as indicated by labels in Fig. 3a. A spectrum averaged over the upper reaction zone region, indicated by dashed lines is shown in Fig. 3b. Strong fluorescence lines are obtained in the reaction zone regions (cf. Fig. 3a) for wavelength ranges 430–440 nm and 460–470 nm corresponding to locations of the (0,16,0) and (0,15,0) vibrational bands reported for NH_2 [12]. In addition, weaker lines also from NH_2 and partially suppressed by the detection filter (GG400, Schott) can be seen at wavelengths 410–420 nm. The identified NH_2 lines were also observed in a spectrum from a corresponding measurement made instead using the dye laser for excitation (data not shown). Fig. 3a and b also show spectral lines from Raman scattering of N_2 and NH_3 at wavelengths 424 and 445 nm, respectively, both showing their strongest signal in the region of unburned reactants (cf. Fig. 3a). An H_2O Raman signal, strongest in the reaction zone regions, is observed at 449 nm. All the spectral lines appear superimposed on a continuous fluorescence background, which will be discussed in the following.

Fig. 3c shows a fluorescence emission spectrum measured in the NH_3-argon jet where NH_2 fluorescence bands can be observed around wavelengths 410, 430 and 460 nm. The spectrum also contains a peak at 336 nm, corresponding to NH (0-0) $A^3\Pi$-$X^3\Sigma^-$ transitions, as well as a strong peak at 385 nm corresponding to elastically scattered laser radiation. The NH_2 region shows a continuous background, which can be seen by comparison with the background level between the NH peak and the laser scattering peak, shown more clearly in the insert of Fig. 3c. Similar to the observations in the excitation scan spectra in Fig. 2 the presence of the continuous background during photolysis indicates that this is a contribution from unresolved spectral line structure of NH_2.

Consequently, NH_2 is also a likely contribution to the continuous background in the fluorescence emission spectra measured in the flame. However, in a flame, contributions from other species with absorption and fluorescence in the investigated spectral regions are also possible. Tuning the laser to 387.2 nm where the excitation spectrum lacks distinct lines results in the dashed spectrum of Fig. 3b, which lacks the NH_2 spectral lines but where the Raman lines and the continuous background remain. Nevertheless, measurements in a premixed CH_4-air flame showed no continuous background while it appeared when seeding the CH_4-air flame with 0.5% NH_3 to the fuel (data not

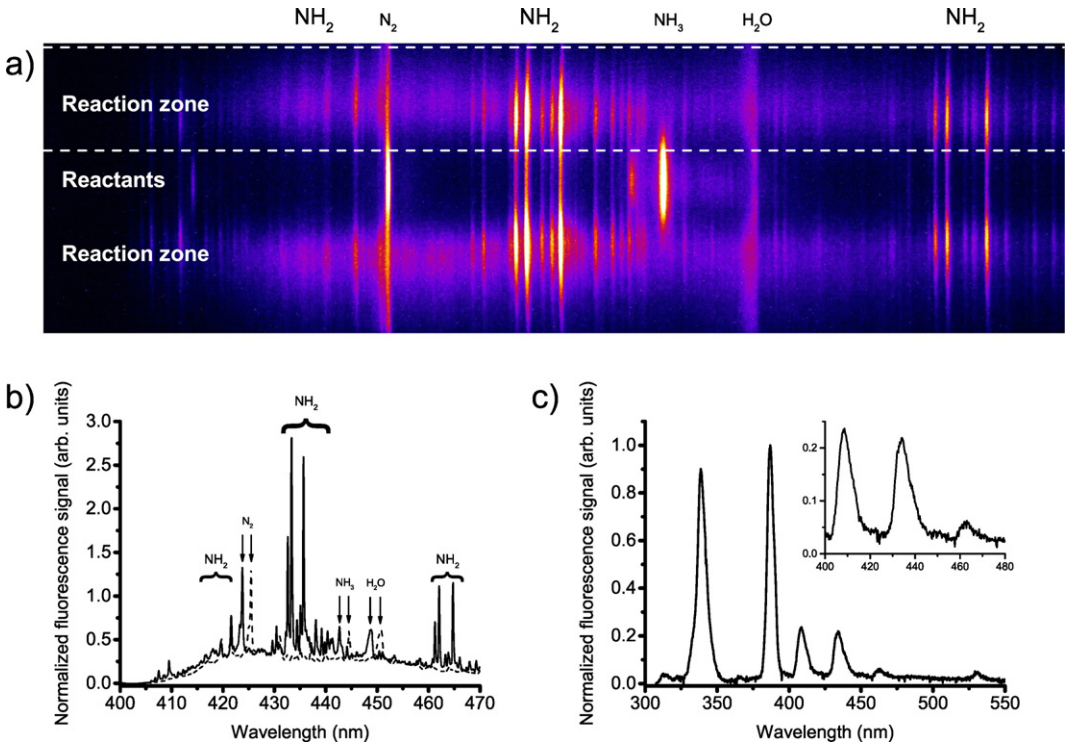

Fig. 3. a) Image of spatially resolved and spectrally dispersed LIF measured in a $\Phi = 1.4$ NH_3-air flame using the Alexandrite laser with excitation at 385.7 nm (arrow in Fig. 2a). Features of NH_2 can be identified in the reaction zone, located at the edges of the flame cone, while the inner side with unburned reactants shows stronger Raman signals from N_2 and NH_3. b) Fluorescence spectra averaged over the reaction-zone region indicated by the white dashed lines in the image in (a) for excitation at 385.7 nm (solid) and 387.2 nm (dashed). NH_2 fluorescence bands around 420, 435 and 460 nm can be identified as well as Raman lines from N_2 (~424 nm), NH_3 (~445 nm), and H_2O (~449 nm). c) Fluorescence spectrum of photolytically produced NH_2 obtained for excitation at 385.7 nm. A peak of elastically scattered laser light is observed at 385 nm together with fluorescence bands from NH (~336 nm) and NH_2 (~435 and ~460 nm).

shown). Thus, it can be concluded that the signal is related to the presence of nitrogen in the fuel and most likely generated by a nitrogen species.

For further analysis of the fluorescence signal and potential contributions, premixed NH_3-air flames of different equivalence ratios were simulated using a kinetic mechanism developed by Mendiara and Glarborg [28]. The simulations were made using a subset of reactions including 31 H/N/O species for one-dimensional free-propagating flames and consequently do not take effects of flame stretching or the CH_4-air pilot flame into account. Fig. 4 shows predicted NH_2 peak number densities together with the average LIF signal measured in premixed NH_3-air flames of different stoichiometry with the dye laser positioned at the line at 385.7 nm (cf. Fig. 2a).

The LIF signal intensity and the NH_2 number density show similar dependence on equivalence ratio, with maxima in the range $\Phi = 1.2$–1.4. To assess potential signal contribution from other nitrogen species, the spectroscopy and equivalence ratio dependence were investigated for species included in the flame chemistry simulations. In the chemical mechanism, nitrogen oxides, radicals such as HNO, HNO_2, and H_2NO, as well as hydrazine (N_2H_4), the hydrazyl radical (N_2H_3), and the diimide (N_2H_2) compound are present at concentration levels of at least tens of ppm. Nitrogen oxide and dinitrogen oxide only exhibit absorption in the UV below 300 nm and are therefore not excited by the laser. Nitrogen dioxide, NO_2, however, has a continuous absorption spectrum from 300 to 600 nm [29,30] thus overlapping with wavelengths for NH_2 excitation. However, this species is dissociated into NO and atomic oxygen for wavelengths below 398 nm [29,31] with a yield that is reported to increase with temperature [32] and thus to be favored in the flame compared with ambient conditions. Moreover, NO_2 is reported not to generate any fluorescence when excited in this wavelength regime [29,31,33] and the concentration is predicted to decrease with increasing flame equivalence ratio at fuel-rich conditions above $\Phi = 1.0$, in contrast to the observed trend for the measured LIF signal (cf. Fig. 4).

The nitroxyl radical, HNO, features absorption at wavelengths in the red and near-infrared region with the electronic transition at 760 nm [34]. Nitrous acid, HNO_2, shows appreciable absorption at the investigated excitation wavelengths [35]. However, the mechanism predicts HNO_2 concentration to decrease with flame equivalence ratio at fuel-rich conditions above $\Phi = 1.0$ and to be about two orders of magnitude lower than those of NH_2. The H_2NO radical exhibits absorption for electronic transitions in the visible regime peaking in the wavelength interval 420–480 nm [36] and vibrational bands of these transitions could potentially extend to the wavelengths employed for NH_2 excitation, however the transitions are reported as weak.

For hydrazine, N_2H_4, absorption at wavelengths below 419.2 nm is reported to dissociate the molecule into two NH_2 fragments, which, however, are created in their ground state and do not directly emit fluorescence [37]. While subsequent excitation of the generated NH_2 fragment in principle is possible, the flame chemistry simulations indicate peak hydrazine concentrations to be one order of magnitude lower than that of NH_2. If present, such a background contribution would therefore most likely be small. The hydrazyl radical, N_2H_3, is reported to have absorption at UV wavelengths 290–400 nm [37,38] while little is known on its fluorescence properties. However, concentration levels are predicted to be one to two orders of magnitude lower than that of NH_2 making it unlikely to be a major contribution to the fluorescence signal. The diimide compound, N_2H_2, is predicted to exist at appreciable concentration levels, a few hundred ppm, and exhibits continuous absorption in the wavelength range 300–430 nm. However, the transitions are of a normally forbidden band resulting in rather weak absorption [31,39,40].

Altogether, it is suggested that the fluorescence signal obtained in the NH_3-air flames for excitation in the 385–390 nm region, including the continuous feature of the emission spectra, is generated by NH_2. Nevertheless, ambiguities related to the continuous background in a flame can be avoided by measurements with the laser tuned on and off the distinct NH_2 rotational lines (cf. Fig. 2a) followed by subtraction of the continuous background (cf. Fig. 3b).

Flame diagnostics of NH_2 by means of LIF has previously been carried out using excitation in the visible regime, for example by Copeland et al. [19]. For direct comparison with that approach, NH_2 excitation was also carried out with the dye laser tuned to 630 nm, probing the $A^2A_1(0,8,0)\Sigma \leftarrow X^2B_1(0,0,0)$ vibrational band. Fluorescence was detected above 650 nm using a long-pass filter (RG645 Schott, AG), resulting in the dashed NH_2 profile presented in Fig. 5.

The dashed NH_2 profile shows very good agreement in shape with a profile measured using the Alexandrite laser tuned to 385.7 nm and shown as a solid curve in Fig. 5. This also confirms NH_2 fluorescence to be the major signal contribution when probing the line at 385.7 nm. The profiles were measured using similar pulse energies for the Alexandrite and dye laser, 35 and 41 mJ, respectively. However, the dashed profile, measured using the dye laser, has been multiplied by a factor of 15 to make it comparable in strength to the solid one, thus indicating a stronger LIF signal for excitation in the (0,19,0) band. The 385 nm excitation alternative with detection around 450 nm is favored by the higher sensitivity of the employed ICCD detector for which the sensitivity is typically a factor of 3 lower at red wavelengths compared with blue. Thus it can be estimated that excitation in the blue regime using the Alexandrite laser was at least a factor of five more efficient compared with excitation at longer wavelengths.

A number of species relevant to combustion, for example the diatomic CH and CN radicals as well as NO_2 have electronic transitions for LIF in the investigated wavelength regime. Thus, care has to be taken for LIF diagnostics in combustion studies involving both nitrogen and hydrocarbon fuel components. The CN B-X (0-0) band has a bandhead degraded towards shorter wavelengths at 388 nm while the (1-0) band is located around 422 nm. Similarly the CH B-X (0-0) band

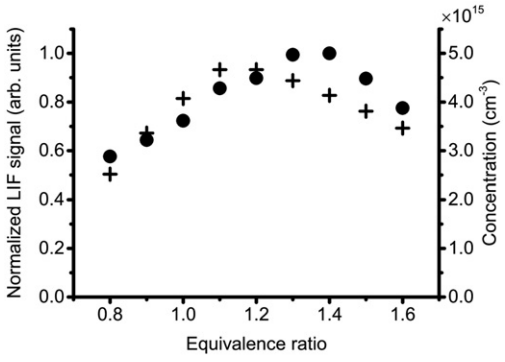

Fig. 4. Fluorescence signal (circles) and calculated number densities of NH_2 (crosses) versus equivalence ratio in premixed NH_3-air flames.

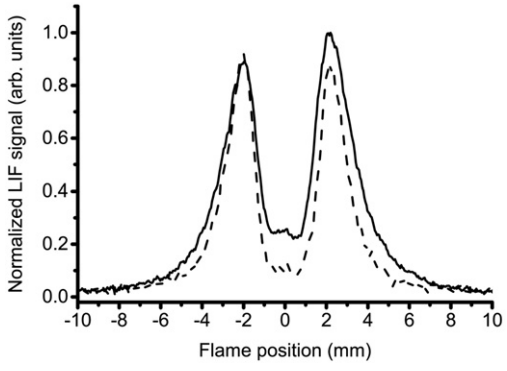

Fig. 5. NH_2 profiles measured in a $\Phi = 1.4$ NH_3-air flame with Alexandrite laser excitation at 385.7 nm (solid) and dye laser excitation at 630 nm (dashed) in the NH_2 $A^2A_1(0,8,0)\Sigma \leftarrow X^2B_1(0,0,0)$ band, the latter similar to the approach of Copeland et al. [19].

is located at 387 nm while the B-X (0-1), A-X (1-1) and A-X (0-0) bands overlap in the spectral range around 431 nm. Excitation at 387 nm and LIF detection at 431 nm has been employed previously for CH measurements using the Alexandrite laser [23]. While the CN B-X (1-0) band at 422 nm that interferes with NH_2 fluorescence can be suppressed by a proper choice of detection filter, the CH fluorescence at 431 nm distinctly overlaps with the NH_2 (0,16,0) band.

An investigation of possible interference was made with measurements in a stoichiometric CH_4-air jet flame with the Alexandrite laser tuned to the CH bandhead at 387.2 nm resulting in CH fluorescence around 431 nm. Addition of 5000 ppm NH_3 to the CH_4-air flame did not result in any distinct NH_2 lines in the fluorescence emission spectrum but a spectrally broad fluorescence contribution background similar to that observed in Fig. 3a was obtained. Thus, compounds generated in fuel-nitrogen chemistry may interfere with fluorescence detection of CH as observed previously [10]. Conversely, a small CH signal was observed in the pure CH_4-air flame for excitation at 385.7 nm, i.e. at the position of the identified NH_2 line and outside the CH B-X (0-0) band. This can possibly be attributed to excitation by the wings of the laser spectral profile, which may give appreciable signal under the relatively tight focusing employed in these measurements.

Under stationary conditions fluorescence interferences can be handled by subtraction of background fluorescence measured off NH_2 resonance, cf. Fig. 3a. For measurements in a single point or along a line spectrally resolved detection is recommended which allows for clear identification of the NH_2 lines also for single-pulse measurements. For single-pulse fluorescence imaging, interference from CN can be avoided using suitable filter, while interference from CH should be low as the laser irradiance level would be sufficiently low to avoid CH excitation due to wing effects as discussed above. In general, it can be concluded that fluorescence interference and cross talk between nitrogen compounds needs to be considered in diagnostics of combustion with fuel-nitrogen conversion.

Fig. 6a shows an NH_2 LIF signal measured with the Alexandrite laser tuned to 385.7 nm, plotted versus laser irradiance. The signal was detected at wavelengths above 400 nm and a background acquired with the laser blocked was subtracted. At irradiances typically below 0.02 GW/cm^2 the signal shows a linear dependence whereas a weaker $I^{0.8}$ trend is observed at higher irradiance levels. The results show that saturated fluorescence is not achieved even for laser pulse energies of 70 mJ focused into a small sheet. Excitation at high energy may, however, induce undesirable photo-chemical effects, which also need to be considered.

Fig. 6b presents two NH_2 profiles measured at laser irradiances 170 and 10 MW/cm^2, corresponding to pulse energies of 70 and 4 mJ, respectively. The profiles have been normalized and show similar NH_2 distributions, however, an additional signal contribution can be seen at position 0 mm in the center for the profile acquired at high irradiance. This signal was present at the burner jet outlet also in a room temperature flow of the fuel and air. Moreover, it showed strong dependence on laser polarization and is therefore attributed to the Raman signals of the unburned mixture in the central region of the flame as shown in the spectral image of Fig. 3a. As shown in Fig. 3a, a small N_2 Raman contribution can be expected also for the regions of NH_2 at opposite sides of the flame center. However, since the signal level approaches zero outside the flame cone, e.g. at position 8 mm in Fig. 6b, where high amounts of N_2 can be expected, an N_2 Raman contribution to the NH_2 signal is small. Thus, the similarity in NH_2 distributions indicates that potential photochemical effects do not have observable impact on the NH_2 signal.

Fig. 7 shows the fluorescence signal-to-noise ratio for NH_2 generated from photolysis in NH_3-Argon mixtures at different NH_3 concentrations. The NH_2 concentrations have been derived from the NH_3 absorption cross section at 213 nm, $\sigma_{abs} = 3 \cdot 10^{-18}$ cm^2 [41], assuming that all absorbed photons result in photo-dissociation generating NH_2. The detection noise was taken as the standard deviation in an image region absent of fluorescence signal. Measurements were made using the dye

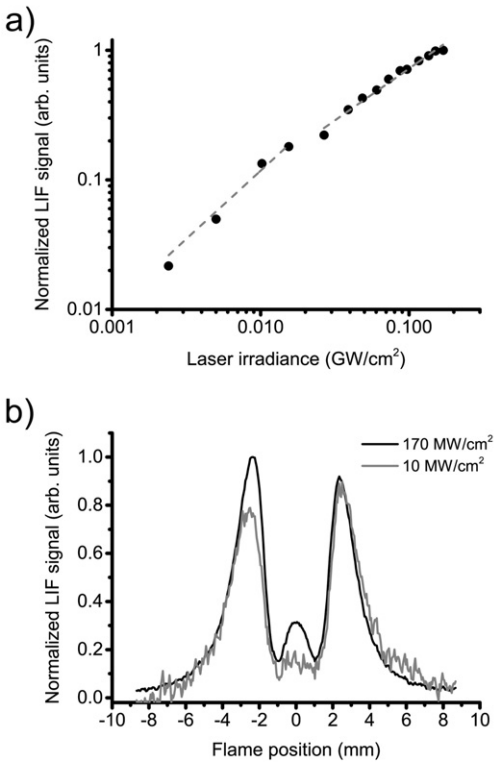

Fig. 6. a) NH_2 LIF signal versus laser irradiance with Alexandrite laser excitation at 385.7 nm. A linear dependence is observed for irradiance levels up to ~0.02 GW/cm^2 whereas a weaker $I^{0.8}$ trend is obtained at higher levels, indicating partial saturation of the signal. b) Normalized NH_2 profiles measured using Alexandrite laser excitation at irradiances of 0.17 (black) and 0.01 (grey) GW/cm^2. The similar shape of the NH_2 peaks on each side of the flame indicates no observable photochemical effects on the detected signal. A Raman signal, discussed in the main text, is observed at the flame center for excitation at the higher irradiance level.

laser exciting the NH_2 line at 385.7 nm with a pulse energy of 8 mJ and the probe volume consisted of a ~4 mm high vertical laser sheet. A signal-to-noise ratio of two is achieved for an NH_2 concentration of around 120 ppm. In flame, for which simulations predict temperatures of 1800–2000 K, the gas number density would be a factor of 6 lower, the signal-to-noise ratio would decrease accordingly, and the detection limit would be around 700 ppm. Laser pulse energies a factor of ~8 higher are available with the Alexandrite laser and allow for improved signal-to-noise ratio with correspondingly reduced detection limit, or imaging measurements as presented in Fig. 8.

Fig. 8 shows sample NH_2 LIF images measured in the $\Phi = 1.4$ NH_3-air flame for Alexandrite laser excitation at 385.7 nm. The images were acquired with a pulse energy of 63 mJ and the beam was shaped

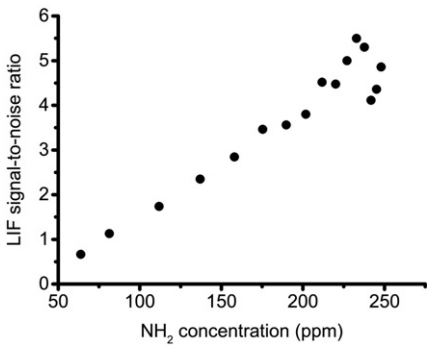

Fig. 7. NH_2 LIF signal-to-noise ratio for excitation at 385.7 nm versus relative concentration of NH_2, generated by UV photolysis, in mixtures of NH_3 and Argon. A signal-to-noise ratio of 2, representing a detection limit, is obtained for 120 ppm NH_2 at room temperature.

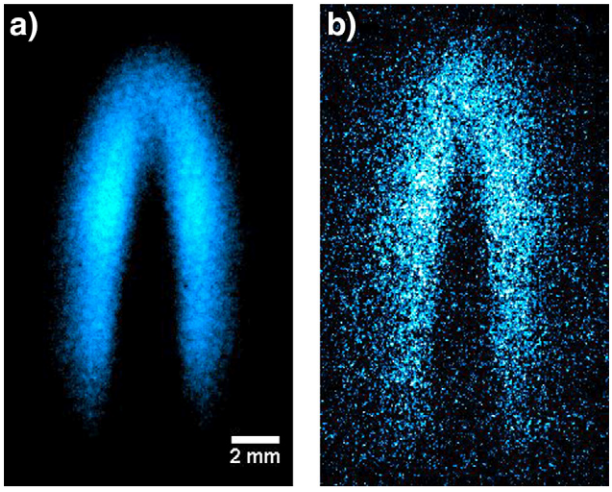

Fig. 8. NH_2 fluorescence images acquired in a $\Phi = 1.4$ NH_3-air flame with Alexandrite laser excitation at 385.7 nm, 100-shot average (a) and single-shot (b) with signal-to-noise ratio ~3.

and focused into a 20 mm high laser sheet covering the flame tip region. The NH_2 distribution is clearly visualized in the image of Fig. 8a, averaged over 100 laser pulses, and a ~2 mm wide NH_2 layer can be observed in the flame tip region. In comparison with the conditions for measurement of NH_2 profiles presented in Fig. 5, the signal obtained on the inner side of the flame cone is lower, as the irradiance level achieved for this arrangement is too low to generate sufficient Raman signals.

Non-stationary conditions require single-shot imaging as exemplified in the image of Fig. 8b with a signal-to-noise ratio of 3. Simulation of a one-dimensional $\Phi = 1.4$ NH_3-air flame predicts a peak NH_2 mole fraction around 1000 ppm and absorption measurements of NH_2 in fuel-rich NH_3-O_2 flames by Chou et al. resulted in peak NH_2 molar fractions around 800 ppm [15]. Assuming a similar NH_2 concentration in the flame imaged in Fig. 8 suggests a detection limit for single-shot imaging at flame conditions of ~700 ppm. This is in agreement with the detection limit for flame conditions estimated in the discussion above. For the images in Fig. 8, the 20 mm measurement volume is about five times larger than that of the photolysis measurements, however, this is compensated by the eight times higher pulse energy, 63 mJ, available with the Alexandrite laser. Therefore, the two estimated detection limits for NH_2 LIF imaging are fairly consistent.

4. Conclusions

Laser-induced fluorescence detection of NH_2 in combustion has been characterized for excitation of the (0,19,0) $A^2A_1 \leftarrow$ (0,0,0) X^2B_1 transition at 385.7 nm. Utilization of the second harmonic of an Alexandrite laser for excitation provides improved NH_2 probing. Excitation at irradiances up to 0.2 GW/cm^2 did not result in fluorescence saturation allowing for efficient utilization of available laser power. Fluorescence excitation spectra showed rotational lines identified as NH_2 but also a broader unresolved continuous feature. Similarly, fluorescence emission spectra showed lines from NH_2 as well as a broad continuous background fluorescence. Investigations suggest that this continuous structure is also generated from NH_2, however, definite NH_2 measurements can be accomplished by having the laser tuned on and off the identified rotational lines. Potential interference from other compounds with absorption and fluorescence in the investigated spectral region has been investigated and in general interference and signal cross-talk need to be considered for fluorescence diagnostics in studies of fuel-nitrogen conversion in combustion. The NH_2 detection limit of 120 ppm at room temperature was achieved for a measurement volume a few millimeters wide, whereas fluorescence imaging on centimeter scale can be achieved for NH_2 concentrations around 700 ppm in a flame.

The Alexandrite laser features a rather broad line width of 2.5 cm^{-1} while a frequency-doubled dye laser can have a linewidth on the order of 0.1 cm^{-1}. Using such a narrowband dye laser would give more efficient excitation of a specific NH_2 line in the investigated spectral region and potentially stronger signal. With increasing irradiance, provided that no detrimental photochemistry is induced, this approach would eventually result in fluorescence saturation, which for many cases is considered to provide strongest signal and best detection sensitivity. However, compared with a typical Nd:YAG + dye laser system the Alexandrite laser features a longer pulse (~70 ns), which possibly allows for multiple excitations during the laser pulse, as demonstrated advantageous for measurements of the CH radical. Thus, an accurate comparison between the Alexandrite laser and a narrowband dye laser system for NH_2 excitation in the 385–390 nm spectral requires further investigations. Altogether, the presented approach for NH_2 detection provides enhanced possibilities for characterization of fuel-nitrogen chemistry in combustion.

Acknowledgements

Financial support from the Knut and Alice Wallenberg Foundation (grant KAW 2015.0294), the Swedish Energy Agency through the CECOST programme, and the European Research Council (ERC) through Advanced Grant 669466-TUCLA is gratefully acknowledged.

References

[1] IEA, Technology Road Map - Bioenergy for Heat and Power, 2012.
[2] J.A. Miller, C.T. Bowman, Mechanism and modeling of nitrogen chemistry in combustion, Prog. Energy Combust. 15 (1989) 287–338.
[3] R.K. Lyon, Thermal Denox, Environ. Sci. Technol. 21 (1987) 231–236.
[4] K. Kohse-Höinghaus, J.B. Jeffries, Applied Combustion Diagnostics, Taylor & Francis, New York, 2002.
[5] R. Wellander, M. Richter, M. Aldén, Time-resolved (kHz) 3D imaging of OH PLIF in a flame, Exp. Fluids 55 (2014).
[6] B.A. Williams, J.W. Fleming, Radical species profiles in low-pressure methane flames containing fuel nitrogen compounds, Combust. Flame 110 (1997) 1–13.
[7] C. Brackmann, B. Zhou, Z.S. Li, M. Aldén, Strategies for quantitative planar laser-induced fluorescence of NH radicals in flames, Combust. Sci. Technol. 188 (2016) 529–541.
[8] B. Zhou, C. Brackmann, Z.S. Li, M. Aldén, Development and application of CN PLIF for single-shot imaging in turbulent flames, Combust. Flame (2014).
[9] Z.W. Sun, Z.S. Li, A.A. Konnov, M. Aldén, Quantitative HCN measurements in CH_4/N_2O/O_2/N_2 flames using mid-infrared polarization spectroscopy, Combust. Flame 158 (2011) 1898–1904.
[10] C. Brackmann, O. Hole, B. Zhou, Z.S. Li, M. Aldén, Characterization of ammonia two-photon laser-induced fluorescence for gas-phase diagnostics, Appl. Phys. B Lasers Opt. 115 (2014) 25–33.
[11] Z.W. Sun, N.J. Dam, Z.S. Li, M. Aldén, NCN detection in atmospheric flames, Combust. Flame 157 (2010) 834–836.
[12] K. Dressler, D.A. Ramsay, The electronic absorption spectra of NH_2 and ND_2, Phil. Trans. R. Soc. A 251 (1959) 553.
[13] J. Xin, H.Y. Fan, I. Ionescu, C. Annesley, S.A. Reid, Fluorescence excitation spectroscopy of the $A^2A_1 \leftarrow X^2B_1$ system of jet-cooled NH_2 in the region 2900–4300 Å, J. Mol. Spectrosc. 219 (2003) 37–44.
[14] R.M. Green, J.A. Miller, The measurement of relative concentration profiles of NH_2 using laser-absorption spectroscopy, J. Quant. Spectrosc. Radiat. 26 (1981) 313–327.
[15] M.S. Chou, A.M. Dean, D. Stern, Laser-absorption measurements on OH, NH, and NH_2 in NH_3/O_2 flames - determination of an oscillator strength for NH_2, J. Chem. Phys. 76 (1982) 5334–5340.
[16] M. Votsmeier, S. Song, D.F. Davidson, R.K. Hanson, Sensitive detection of NH_2 in shock tube experiments using frequency modulation spectroscopy, In. J. Chem. Kinet. 31 (1999) 445–453.
[17] I. Rahinov, A. Goldman, S. Cheskis, Absorption spectroscopy diagnostics of amidogen in ammonia-doped methane/air flames, Combust. Flame 145 (2006) 105–116.
[18] M.C. Branch, M.E. Sadeqi, A.A. Alfarayedhi, P.J. van Tiggelen, Measurements of the structure of laminar, premixed flames of CH_4/NO_2/O_2 and CH_2O/NO_2/O_2 mixtures, Combust. Flame 83 (1991) 228–239.
[19] R.A. Copeland, D.R. Crosley, G.P. Smith, Laser-induced Fluorescence Spectroscopy of NCO and NH_2 in Atmospheric Pressure Flames, Twentieth Symposium (International) on Combustion, 20, 1984 1195–1203.
[20] K.N. Wong, W.R. Anderson, J.A. Vanderhoff, A.J. Kotlar, Kr^+ laser excitation of NH_2 in atmospheric-pressure flames, J. Chem. Phys. 86 (1987) 93–101.
[21] C. Brackmann, J. Nygren, B. Xiao, Z. Li, H. Bladh, B. Axelsson, I. Denbratt, L. Koopmans, P.-E. Bengtsson, M. Aldén, Laser-induced fluorescence of formaldehyde in

combustion using third harmonic Nd:YAG laser excitation, Spectrochim. Acta A 59 (2003) 3347–3356.
[22] Z.S. Li, M. Afzelius, J. Zetterberg, M. Aldén, Applications of a single-longitudinal-mode alexandrite laser for diagnostics of parameters of combustion interest, Rev. Sci. Instrum. 75 (2004) 3208–3215.
[23] Z.S. Li, J. Kiefer, J. Zetterberg, M. Linvin, A. Leipertz, X.S. Bai, M. Aldén, Development of improved PLIF CH detection using an Alexandrite laser for single-shot investigation of turbulent and lean flames, Proc. Combust. Inst. 31 (2007) 727–735.
[24] B. Zhou, J. Kiefer, J. Zetterberg, Z.S. Li, M. Aldén, Strategy for PLIF single-shot HCO imaging in turbulent methane/air flames, Combust. Flame 161 (2014) 1566–1574.
[25] C. Jungen, K.E.J. Hallin, A.J. Merer, Orbital angular-momentum in triatomic-molecules II. Vibrational and K-type rotational structure, and intensity factors in the A^2A_1-X^2B_1 transitions of NH_2 and H_2O^+, Mol. Phys. 40 (1980) 25–63.
[26] C.M. Western, PGOPHER, a Program for Simulating Rotational Structure, University of Bristol, 2010.
[27] F.W. Birss, D.A. Ramsay, S.C. Ross, C. Zauli, Molecular-constants for the ground-state of NH_2, J. Mol. Spectrosc. 78 (1979) 344–346.
[28] T. Mendiara, P. Glarborg, Ammonia chemistry in oxy-fuel combustion of methane, Combust. Flame 156 (2009) 1937–1949.
[29] Y. Matsumi, S. Murakami, M. Kono, K. Takahashi, M. Koike, Y. Kondo, High-sensitivity instrument for measuring atmospheric NO_2, Anal. Chem. 73 (2001) 5485–5493.
[30] M.F. Merienne, A. Jenouvrier, B. Coquart, The NO_2 absorption-spectrum I. Absorption cross-sections at ambient-temperature in the 300–500 nm region, J. Atmos. Chem. 20 (1995) 281–297.
[31] H. Okabe, Photochemistry of Small Molecules, Wiley, New York, 1978.
[32] J.G. Calvert, S. Madronich, E.P. Gardner, J.A. Davidson, C.A. Cantrell, R.E. Shetter, Mechanism of NO_2 photodissociation in the energy-deficient region at 404.7 nm, J. Phys. Chem. - Us 91 (1987) 6339–6341.
[33] E.K.C. Lee, W.M. Uselman, Molecular predissociation of nitrogen-dioxide studied by fluorescence excitation spectroscopy, Faraday Discuss. 53 (1972) 125–131.
[34] R.N. Dixon, C.A. Rosser, The characterization of the complete set of bound Vibronic states of HNO in its excited A^1A'' electronic state, J. Mol. Spectrosc. 110 (1985) 262–276.
[35] R. Vasudev, Absorption-spectrum and solar photodissociation of gaseous nitrous-acid in the actinic wavelength region, Geophys. Res. Lett. 17 (1990) 2153–2155.
[36] A. Ricca, J. Weber, M. Hanus, Y. Ellinger, The shape of the ground and lowest 2 excited-states of H_2NO, J. Chem. Phys. 103 (1995) 274–280.
[37] G.L. Vaghjiani, Ultraviolet-absorption cross-sections for N_2H_4 vapor between 191–291 nm and $H(^2S)$ quantum yield in 248 nm photodissociation at 296 K, J. Chem. Phys. 98 (1993) 2123–2131.
[38] M. Arvis, C. Deviller, M. Gillois, M. Curtat, Isothermal flash-photolysis of hydrazine, J. Phys. Chem. - Us 78 (1974) 1356–1360.
[39] R.A. Back, D.A. Ramsay, C. Willis, Near-ultraviolet absorption-spectrum of diimide vapor, Can. J. Chem. 52 (1974) 1006–1012.
[40] R.A. Back, C. Willis, D.A. Ramsay, Near-ultraviolet absorption-spectrum of diimide - re-examination, Can. J. Chem. 56 (1978) 1575–1578.
[41] B.M. Cheng, H.C. Lu, H.K. Chen, M. Bahou, Y.P. Lee, A.M. Mebel, L.C. Lee, M.C. Liang, Y.L. Yung, Absorption cross sections of NH_3, NH_2D, NHD_2, and ND_3 in the spectral range 140–220 nm and implications for planetary isotopic fractionation, Astrophys. J. 647 (2006) 1535–1542.